Localized subduction of anthropogenic carbon dioxide in the Southern Hemisphere oceans

Jean-Baptiste Sallée[1]*, Richard J. Matear[2], Stephen R. Rintoul[2,3] and Andrew Lenton[2]

The oceans slow the rate of climate change by absorbing about 25% of anthropogenic carbon dioxide emissions annually. The Southern Ocean makes a substantial contribution to this oceanic carbon sink: more than 40% of the anthropogenic carbon dioxide in the ocean has entered south of 40° S. The rate-limiting step in the oceanic sequestration of anthropogenic carbon dioxide is the transfer of carbon across the base of the surface mixed layer into the ocean interior, a process known as subduction. However, the physical mechanisms responsible for the subduction of anthropogenic carbon dioxide are poorly understood. Here we use observationally based estimates of subduction and anthropogenic carbon concentrations in the Southern Ocean to determine the mechanisms responsible for carbon sequestration. We estimate that net subduction amounts to 0.42 ± 0.2 Pg C yr^{-1} between 35° S and the marginal sea-ice zone. We show that subduction occurs in specific locations as a result of the interplay of wind-driven Ekman transport, eddy fluxes and variations in mixed-layer depth. The zonal distribution of the estimated subduction is consistent with the distribution of anthropogenic carbon dioxide in the ocean interior. We conclude that oceanic carbon sequestration depends on physical properties, such as mixed-layer depth, ocean currents, wind and eddies, which are potentially sensitive to climate variability and change.

A tmospheric CO_2 continues to rise at unprecedented rates in response to human activities[1]. At present, the oceans take up more than 25% of anthropogenic CO_2 (C_{ant}) emissions, thereby slowing the growth of atmospheric CO_2 and the rate of climate change[2]. The rate-limiting step for ocean sequestration of C_{ant} is the transfer from the surface ocean to the ocean interior[3–5]. Knowledge of the mechanisms responsible for the transfer of C_{ant} between the well-ventilated surface mixed layer and the ocean interior, and their sensitivity to change, is key to understanding past, present and future carbon uptake by the ocean. However, both the pathways and rate by which C_{ant} is sequestered in the ocean interior remain uncertain. No direct observations of the pathways and rates of anthropogenic carbon sequestration have been made and consequently our present understanding is based on the interior distribution of C_{ant} (ref. 6) or inferred from model simulations[7].

The Southern Ocean is a particularly important region for the uptake and storage of C_{ant} (refs 8,9). The latitude band between 30° S and 50° S stores more C_{ant} than any other latitude band in the ocean[6]. The efficient uptake and storage of C_{ant} by the Southern Ocean is a result of the vigorous overturning circulation at high southern latitudes, in which water masses are formed and subducted into the ocean interior[10]. As water masses sink from the sea surface, they carry C_{ant} into the ocean interior. Sub-Antarctic Mode Water and Antarctic Intermediate Water formed on the northern flank of the Antarctic Circumpolar Current (ACC) make the largest contribution to the uptake and storage of C_{ant} by the Southern Ocean[6,11,12].

Previous studies of the Southern Ocean C_{ant} budget have focussed on air–sea fluxes and vertical transfer by Ekman pumping, with other physical processes transporting C_{ant} into (and out of) the ocean interior either simplified or neglected[13–16]. Three physical processes contribute to the transfer of fluid between the surface mixed layer and the interior ocean: wind-driven Ekman pumping, eddy fluxes and lateral induction by the mean flow. Until recently,

the contribution of eddies and the mean flow to subduction could not be estimated from the available observations. The broad-scale, year-round sampling of the Southern Ocean by Argo floats means that this is now possible[17] (see Methods). Here we show that C_{ant} leaves the ventilated surface layer of the Southern Ocean through localized maxima of subduction and identify the physical mechanisms responsible.

Mechanism of anthropogenic carbon subduction

Here we consider the region between 35° S and the northern limit of the Antarctic winter sea ice ($\approx$65° S), for which there is good Argo coverage. We use recent observationally based estimates of subduction[17] and C_{ant} (ref. 18) in and at the base of the winter mixed layer (Fig. 1a) to calculate the total subduction of C_{ant} from the mixed layer into the ocean interior in the 1990s. We quantify the individual contributions of Ekman divergence, eddy fluxes and the mean flow to subduction (see Methods).

Ekman transport leads to more or less zonally uniform subduction of C_{ant} north of the ACC and reventilation (transport of C_{ant} from below the mixed layer into the mixed layer) south of the ACC (Fig. 1b). The eddy contribution mostly compensates the Ekman transport, with subduction in and south of the ACC and reventilation to the north (Fig. 1d). The mean flow subducts fluid into the interior where the mixed layer shoals along the direction of the surface flow (streamlines) and reventilates fluid where the mixed layer deepens in the direction of the flow, a process known as lateral induction (see Supplementary Information). The mean flow largely determines the regional pattern of subduction and reventilation, which varies strongly from region to region (Fig. 1c). The total transport shows regions of both subduction and reventilation in all three basins (Fig. 1e).

Our calculation gives a total of 0.42 ± 0.2 Pg C yr^{-1} of C_{ant} subducted into the Southern Ocean interior. Zonally averaged,

[1]British Antarctic Survey, High Cross, Madingley Road, Cambridge CB3 0ET, UK, [2]CMAR-CSIRO, Castray Esplanade, Hobart 7000, Tasmania, Australia,
[3]Antarctic Climate and Ecosystems Cooperative Research Centre, Centenary Building, Grosvenor Crescent, Sandy Bay 7005, Tasmania, Australia.
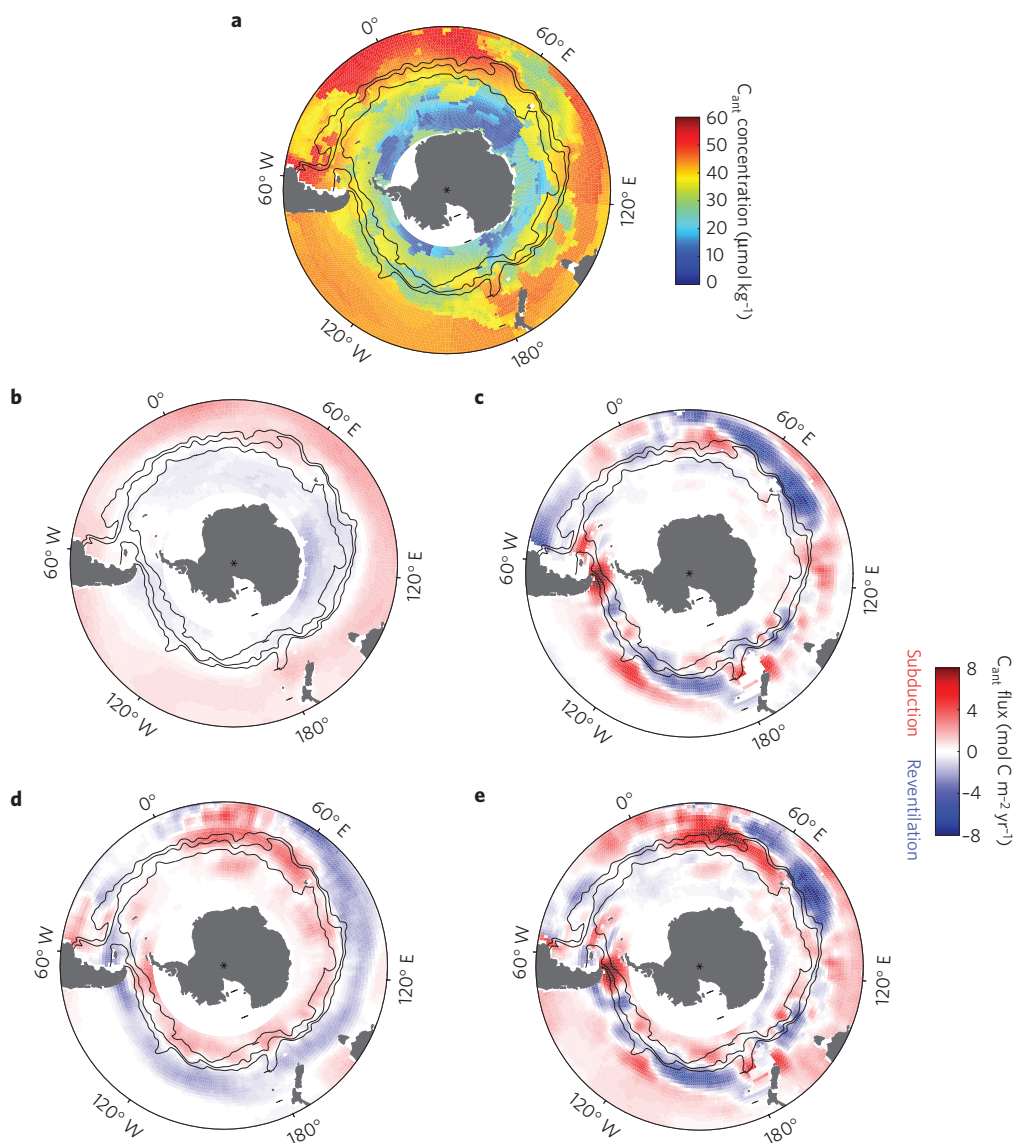*e-mail: jbsallee@gmail.com.

Figure 1 | C_{ant} subduction into the ocean interior. a, Annual mean anthropogenic carbon at the base of the winter mixed layer from the Global Data Analysis Project (ref. 18). The C_{ant} transport out of (+) and into (−) the ventilated surface layer for **b**, Ekman, **c**, mean-flow, **d**, eddy-induced and **e**, total transports. The thin black lines show the mean position of the three main Antarctic Circumpolar Current (ACC) fronts[32] where the most northern and southern lines denote the boundary of the ACC region referred to in Table 1.

most subduction of C_{ant} occurs to the north of the ACC (0.24 ± 0.12 Pg C yr^{-1}; Table 1), reflecting the strong subduction by Ekman transport, partially offset by the eddy fluxes and mean flow. South of the ACC, the reventilation of C_{ant} by the Ekman transport is counter-balanced by subduction induced by eddy transport.

Notably, the zonal averages hide the fact that C_{ant} is both subducted and reventilated in the Southern Ocean. The largest reventilation occurs in the Indian Ocean sector, in a band extending eastwards from South Africa to the middle of the basin. Maxima in reventilation also occur in the Pacific, east of New Zealand, and in the Atlantic, east of South America. Each of these maxima correspond to locations where the outflow from subtropical western boundary currents merges with the ACC and the mixed layer deepens along the direction of the mean flow (streamlines in Fig. 1; see Supplementary Information).

In the reventilation regions, previously subducted C_{ant} is returned to the surface mixed layer. The return of the C_{ant} to the surface mixed layer reduces the efficiency of C_{ant} uptake by the Southern Ocean. Notably, reventilation alters the pathways

by which C_{ant} is transported from the surface mixed layer into the ocean. The connection between subduction and reventilation regions can be either local or remote. If the reventilation region is located directly downstream of the subduction region, and in the same density range, there is little net C_{ant} transport into the ocean. For example, in the western Indian sector a strong reventilation region (40° E–90° E) lies downstream of a strong subduction region (0°–60° E), resulting in weak net subduction (Fig. 1e). The Indian section has regions of strong subduction and reventilation and overall has net subduction of C_{ant} (0.10 Pg C yr^{-1}; Table 1). The net subduction of C_{ant} is slightly stronger in the Pacific (0.18 Pg C yr^{-1}) and Atlantic (0.13 Pg C yr^{-1}) sectors of the Southern Ocean (Table 1).

The error estimates of the C_{ant} transports are mainly owing to the uncertainty in the C_{ant} concentrations. The C_{ant} concentrations used here are empirically derived estimates from measured *in situ* water properties[19] and then mapped to a uniform grid[18]. The C_{ant} concentration estimate has substantial uncertainties[20] because it requires extracting the small anthropogenic carbon signal from the much

Table 1 | Calculated anthropogenic carbon flux through the base of the ventilated surface layer in Pg C yr^{-1} for the year 1995.

Southern Ocean	Total (Pg C yr^{-1})	Ekman (Pg C yr^{-1})	Eddy induced (Pg C yr^{-1})	Mean flow (Pg C yr^{-1})
35°–65° S	0.42 ± 0.2	0.33 ± 0.06	0.11 ± 0.07	−0.02 ± 0.08
North ACC	0.24 ± 0.12	0.49 ± 0.03	−0.24 ± 0.04	−0.0064 ± 0.05
Within ACC	0.1 ± 0.05	−0.01 ± 0.0074	0.15 ± 0.02	−0.04 ± 0.02
South ACC	0.08 ± 0.04	−0.16 ± 0.02	0.21 ± 0.0099	0.02 ± 0.0082
40°–65° S	0.23 ± 0.15			
Basin breakdown: Atlantic				
35°–65° S	0.13 ± 0.04	0.08 ± 0.01	0.1 ± 0.01	−0.05 ± 0.02
North ACC	0.09 ± 0.02	0.12 ± 0.0056	0.03 ± 0.0061	−0.06 ± 0.0096
Within ACC	0.04 ± 0.01	0.0062 ± 0.0013	0.03 ± 0.0045	0.0057 ± 0.0044
South ACC	0.003 ± 0.01	−0.04 ± 0.0058	0.04 ± 0.0028	0.001 ± 0.0029
40°–65° S	0.08 ± 0.03			
Indian				
35°–65° S	0.1 ± 0.12	0.13 ± 0.03	0.05 ± 0.04	−0.08 ± 0.04
North ACC	0.05 ± 0.07	0.23 ± 0.01	−0.15 ± 0.03	−0.04 ± 0.03
Within ACC	0.05 ± 0.02	0.0052 ± 0.0039	0.09 ± 0.0074	−0.05 ± 0.01
South ACC	0.01 ± 0.02	−0.1 ± 0.01	0.1 ± 0.0049	0.01 ± 0.0034
40°–65° S	0.02 ± 0.08			
Pacific				
35°–65° S	0.18 ± 0.04	0.11 ± 0.0098	−0.03 ± 0.01	0.1 ± 0.02
North ACC	0.11 ± 0.02	0.15 ± 0.0064	−0.12 ± 0.0092	0.08 ± 0.0091
Within ACC	0.01 ± 0.01	−0.02 ± 0.0022	0.03 ± 0.0033	0.0075 ± 0.0071
South ACC	0.06 ± 0.0053	−0.01 ± 0.0012	0.06 ± 0.0022	0.01 ± 0.0019
40°–65° S	0.13 ± 0.04			

The physical transport of C_{ant} is given for different zones and sectors of the Southern Ocean (positive value—out of the ventilated surface layer into the ocean interior; negative value—into the ventilated surface layer). The error bars are based on one standard deviation in the C_{ant} concentrations (See Supplementary Information). South ACC is the region between 65° S and the polar front (that is, south of the southern streamline in Fig. 1). The AAC zone is the region between the polar front and the northern branch of the sub-Antarctic Front (that is, between the southern and northern extremes of the streamlines in Fig. 1). North ACC is the region between the northern branch of the sub-Antarctic front and 35° S (that is, north of the northern streamline in Fig. 1). For ease of reading, numbers are rounded to the nearest second decimal. However, numbers smaller than 0.01 have additional significant figures.

larger measured total dissolved inorganic carbon concentration. This substantial uncertainty is particularly large for the Southern Ocean[9], where estimates of C_{ant} diverge even when applied to the same data[21–23]. The C_{ant} concentrations used here are probably uncertain by up to ±40% reflecting uncertainties in estimating C_{ant} (ref. 20) and uncertainties owing to mapping the concentrations to a uniform grid[18] (see Supplementary Information).

Although the uncertainty in C_{ant} concentration influences the magnitude of the net transport of C_{ant} into the ocean interior, it has no impact on the spatial distribution of the subduction and reventilation areas as these are set by the physical transport. Furthermore, the regional distribution of subduction and reventilation sets the pathways by which C_{ant} is transferred from the mixed layer into the ocean interior. We next show that the inferred pathways are consistent with the regional pattern of C_{ant} in the ocean interior.

Surface-to-interior pathways

For effective sequestration, C_{ant} subducted across the base of the mixed layer must be transported into the ocean interior, away from reventilation regions where C_{ant} can be returned to the mixed layer. The transport into the interior is accomplished by advection and mixing, primarily along isopycnal surfaces. Although isopycnal mixing has a significant impact on transport in the ocean interior[24], its contribution to subduction is negligible because it acts only at the base of the ventilated surface layer (see Methods). The inventory of C_{ant} in the thermocline should therefore reflect the regional

distribution of subduction and the isopycnal transport of C_{ant} in the ocean interior.

The distribution of C_{ant} in the ocean interior is consistent with this hypothesis (Fig. 2). Maxima in the observed inventory of C_{ant} occur in regions of strong net subduction and spread equatorwards along streamlines into the ocean interior. For example, significant amounts of C_{ant} are found on the potential density $\sigma_\theta = 26.8$ surface in the Indian Ocean, spreading equatorwards along mean streamlines from the strong subduction region in the southeastern part of the basin, which is consistent with the distribution of potential vorticity[17]. Similarly, significant inventories of C_{ant} are found in the Pacific on the $\sigma_\theta = 27.0$ surface and in the Atlantic on the $\sigma_\theta = 27.2$ surface. C_{ant} is injected on the $\sigma_\theta = 27.1$ surface near the Drake Passage and spreads into both the Pacific and Atlantic basins. The strong regional variations in the oceanic inventory of C_{ant} reflect the distribution of subduction hotspots and the circulation patterns linking these subduction regions with the ocean interior.

The inventory of C_{ant} in density layers at 30° S reveals the dominant pathways by which C_{ant} is exported from the Southern Ocean to the subtropical gyres (Fig. 3). In the lightest density classes ($\sigma_\theta = 26.7$–26.9), most of the C_{ant} inventory is located in the Indian Ocean, particularly east of 60° E, consistent with our estimated transport through the base of the surface layer (Fig. 2a,b). Between $\sigma_\theta = 26.9$ and 27.1, the Pacific makes the dominant contribution to the inventory of C_{ant}, with the largest values in the central basin (Fig. 2). The Atlantic sequesters the greatest amount of C_{ant} in the
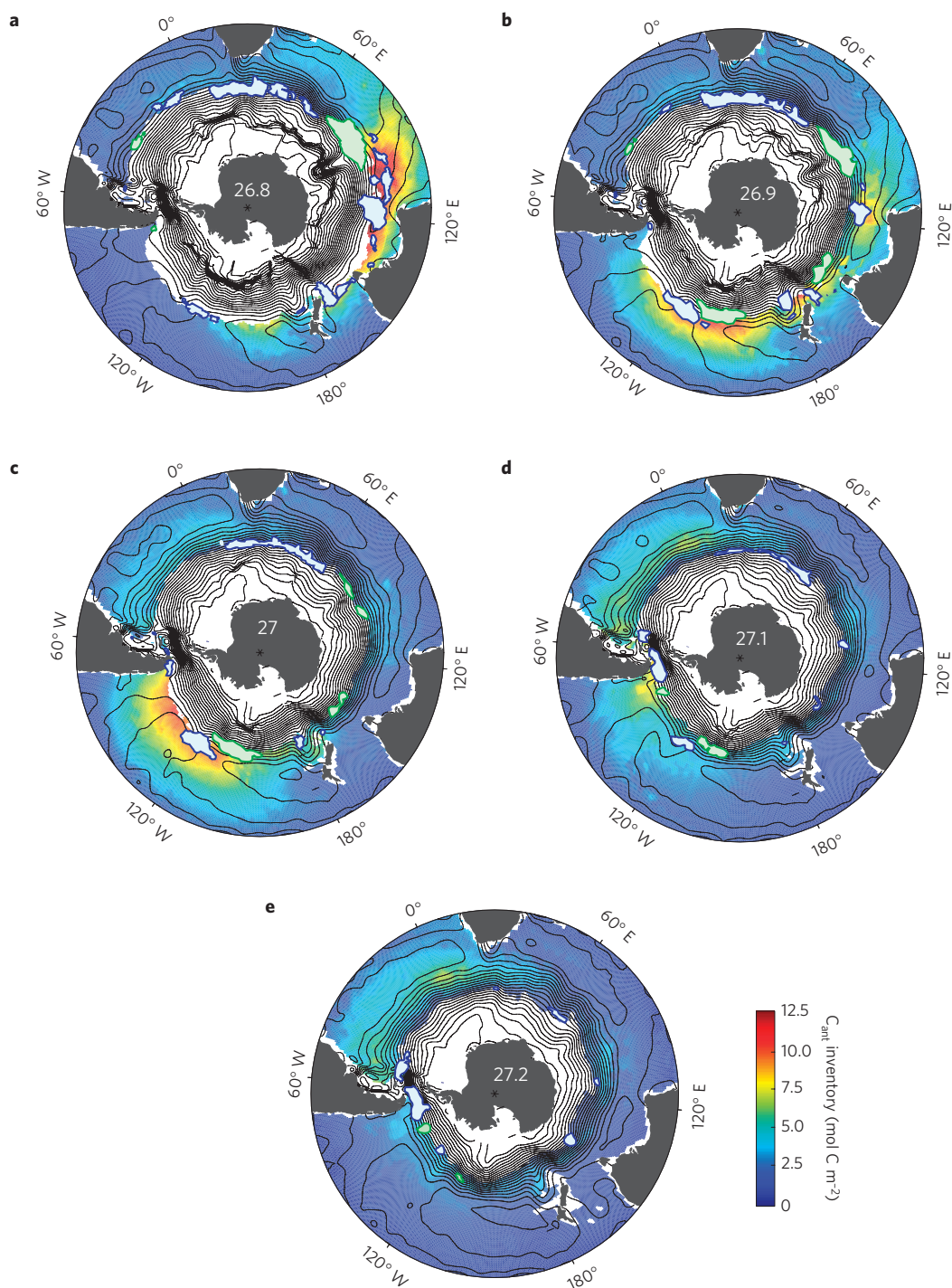
Figure 2 | C_{ant} inventory versus subduction pattern. The C_{ant} inventory on selected isopycnal surfaces ($\pm 0.05\sigma_\theta$): **a**, 26.8, **b**, 26.9, **c**, 27, **d**, 27.1 and **e**, 27.2. The black lines are the Montgomery streamlines indicating the approximate geostrophic circulation on each isopycnal. White patches highlighted with a thick blue line are regions of subduction maxima. White patches with a thick green line are regions of reventilation maxima.

density range of the Antarctic Intermediate Water ($\sigma_\theta = 27.0$–27.4), although C_{ant} is present at lighter densities as well. The highest values are found on the western side of the basin, consistent with subduction in Drake Passage.

Uptake of of anthropogenic carbon

Our estimate of the net subduction of C_{ant} into the ocean interior ($0.42\,\mathrm{Pg\,C\,yr^{-1}}$ in 1995 between 35° and 65° S) is smaller than estimates of the Southern Ocean uptake of C_{ant} across the air–sea interface ($\approx 0.8\,\mathrm{pg\,C\,yr^{-1}}$; refs 8,9), underscoring the fact that

transfer across the base of the mixed layer is the rate-limiting step in the sequestration of C_{ant} in the ocean interior. We compute the total sequestration of C_{ant} by net subduction since 1800, by assuming the physical volume transport has not changed over the past two centuries, while accounting for the temporal evolution of C_{ant} in the surface mixed layer (see Supplementary Information). We estimate that $23 \pm 10\,\mathrm{Pg\,C}$ of C_{ant} was sequestered between 1800 and 1995. From the Global Data Analysis Project product[18], we calculate a total inventory of $25 \pm 5\,\mathrm{Pg\,C}$ for the Southern Hemisphere between density layers 26.0 and 27.8 kg m^{-3}.
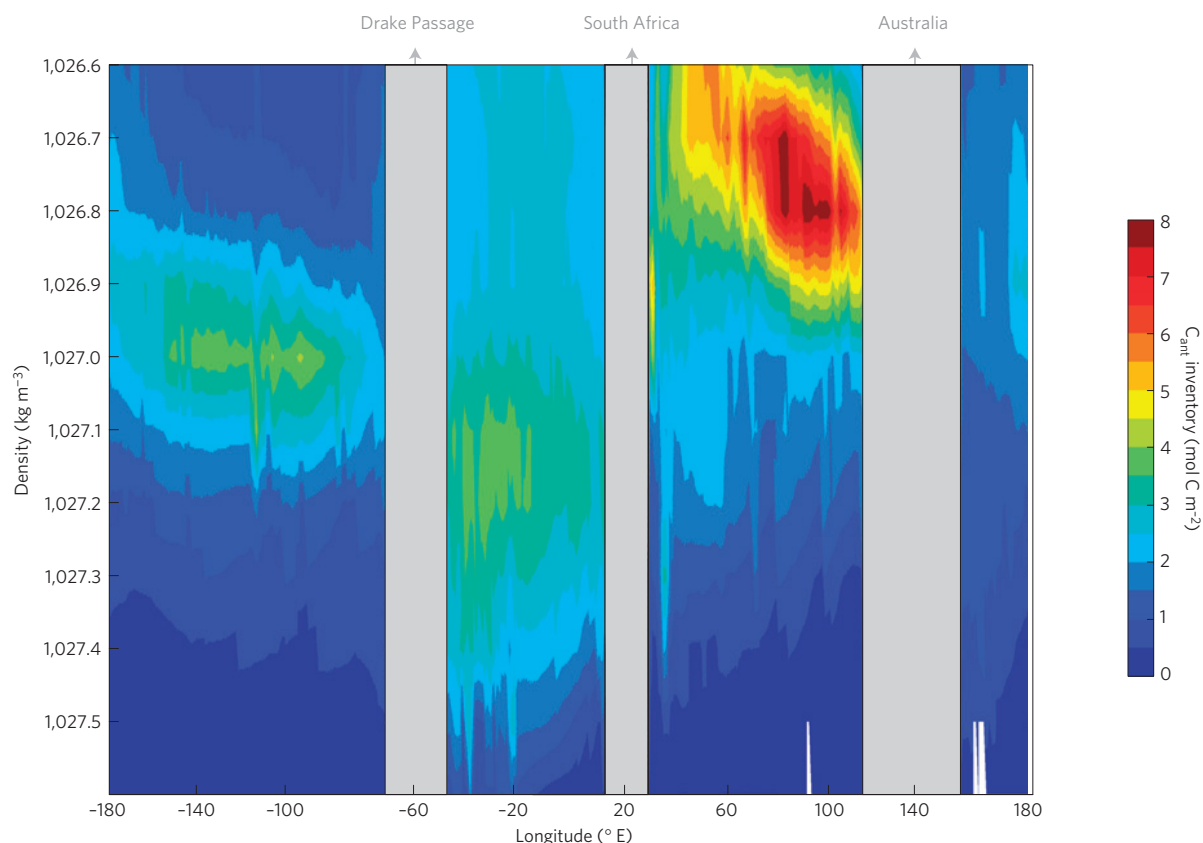
Figure 3 | Vertical structure of C$_{ant}$ inventory at 30° S. Circumpolar section of C$_{ant}$ inventory at 30° S along potential density surfaces (inventory within ±0.05σ_θ).

Our estimate of the net subduction of C$_{ant}$ in the Southern Ocean is therefore consistent with the estimated inventory of C$_{ant}$ in the ocean interior.

The subduction estimate can be combined with other information to compute an overall budget for C$_{ant}$ for comparison with previous studies of the oceanic uptake of C$_{ant}$ south of 40° S. Our net subduction of C$_{ant}$ between 65° and 40° S was 0.23 ± 0.15 Pg C yr^{-1} in 1995. We estimate the accumulation rate of C$_{ant}$ in the mixed layer to be 0.16 ± 0.16 Pg C yr^{-1} in 1995, based on measurements of the depth of the mixed layer and the observed rate of increase of dissolved inorganic carbon in the surface layer (see Supplementary Information). An ocean carbon model was used in a previous study[7] to estimate a northward transport across 40° S within the mixed layer of 0.16 Pg C yr^{-1}. The sum of these contributions implies a net air–sea uptake of C$_{ant}$ of 0.55 ± 0.31 Pg C yr^{-1} between 40° S and the sea-ice zone (65° S). This value is consistent with recent independent estimates of the air–sea exchange of C$_{ant}$ south of 40° S based on a Green's function approach (0.8 ± 0.2 Pg C yr^{-1}; refs 8,9), of which 0.1–0.2 Pg C yr^{-1} probably occurs in the sea-ice zone, which is not included in our calculation.

C$_{ant}$ enters the ocean in specific locations and spreads equatorwards along well-defined transport pathways, rather than uniformly around the circumpolar belt. Physical transport processes in the Southern Ocean also reventilate C$_{ant}$ contained in the ocean interior, hence estimates of net sequestration must therefore account for both the subduction and reventilation of C$_{ant}$. Two often neglected physical mechanisms—eddy transport and lateral induction by the mean flow—make a significant contribution to the magnitude and distribution of the subduction of C$_{ant}$ and must be considered when investigating the upper-ocean carbon budget. This is shown in a recent modelling study, where lateral induction was an important contributor to the subduction of total carbon[25]. Our analysis

demonstrates that the subduction of C$_{ant}$ in the Southern Ocean depends on physical variables that are sensitive to climate variability and change, including wind stress, eddy fluxes, surface currents and mixed-layer depth. Present climate models vary widely in their ability to represent these properties[26,27] and therefore the present and future subduction of C$_{ant}$. Our results provide an observationally based estimate of the spatial distribution and magnitude of C$_{ant}$ transport from the surface to the ocean interior that can be used to assess models.

Methods

We define the physical transport of C$_{ant}$ out of the upper ocean into the ocean interior as the rate by which C$_{ant}$ is injected from the seasonal thermocline (that is, the water above the base of the winter mixed layer, which has been in recent contact with the atmosphere) into the ocean interior[17]. This transport is associated with the C$_{ant}$ budget above the base of the winter mixed layer:

$$\frac{\partial C_{ant}}{\partial t} + \nabla \cdot [T_{res}(t) \cdot C_{ant}(t)] = \mathcal{C}_{uptake} \qquad (1a)$$

which becomes after time averaging:

$$\underbrace{\overline{C_{ant} \cdot \bar{S}} + \mathcal{M}_{base\ SL}}_{C_{subduction}} = \overline{\mathcal{C}_{uptake}} - \overline{\mathcal{C}_{acc}} - \underbrace{(\overline{T_{res} \cdot \nabla_h \overline{C_{ant}}} + \mathcal{M}_{SL})}_{horizontal\ transport}, \qquad (1b)$$

where $\overline{(.)}$ refers to the annual mean; T_{res} is the transport above the base of the winter mixed layer resulting from the Ekman, mean and eddy-induced flow; $\bar{S} = \nabla_h \overline{T_{res}}$ is the annual mean subduction[17]; $\overline{\mathcal{C}_{uptake}}$ is the annual mean air–sea flux of C$_{ant}$; $\overline{\mathcal{C}_{acc}}$ is the annual mean C$_{ant}$ accumulation in the surface layer; $\mathcal{M}_{base\ SL}$ is the mixing term operating at the base of the surface layer; and $\mathcal{M}_{SL}$ is the horizontal mixing operating within the mixed layer; t is time; $\nabla \cdot$ is the divergence operator; and ∇_h is the horizontal gradient operator.

We define subduction as the transport of C$_{ant}$ out of the ventilated surface layer into the ocean interior and reventilation as the transport of C$_{ant}$ from the ocean interior back into the ventilated surface layer. This two-way transfer of C$_{ant}$ across the base of the winter mixed layer, C$_{subduction}(t)$, can occur all

year round and is the result of the divergence of C_{ant} transport within the ventilated layer and mixing processes at the base of the surface layer (left-hand side of equation (1b)).

Our calculation is applied in the Southern Ocean, north of the marginal sea-ice zone where the Argo coverage provides sufficient observations. The estimates of annual mean water mass injection into the ocean interior ($\bar{S}$) agree with the climatological potential vorticity structure of the ocean interior[17].

The mixing term in the left-hand side of equation (1b) includes a vertical mixing term at the base of the surface layer and an along-isopycnal eddy flux[28,29]:

$$\mathcal{M}_{base\,SL} = \int_{surface-layer} \left(\frac{\partial}{\partial z} \kappa_z \frac{\partial C}{\partial z} + \nabla_\gamma \cdot \kappa_\gamma \nabla_\gamma C \right) \cdot dz \quad (2)$$

where z is depth, κ_z and κ_γ are the vertical and along-isopycnal mixing coefficients and ∇_γ and ($\nabla_\gamma \cdot$) are the along-isopycnal gradient and divergence operator. Because C_{ant} is well mixed in the surface layer (that is, $\partial C/\partial z = \nabla_\gamma C = 0$), the mixing terms act only at the base of the surface layer. An upper-bound estimate of the magnitude of the mixing terms can be made using large mixing coefficients[30,31] ($\kappa_z \propto 10^{-4}$ m² s⁻¹ and $\kappa_\gamma \propto 10^4$ m² s⁻¹) and conservative values of the gradient of C_{ant} (10 µmol kg⁻¹ over 50 m depth and 10 µmol kg⁻¹ over 1° on isopycnals). Therefore, the vertical mixing term is estimated to be 10^{-17} Pg C m⁻² yr⁻¹ and the isopycnal mixing term to be 10^{-15} Pg C m⁻² yr⁻¹, which are two orders of magnitude smaller than the other terms (Fig. 1) and are neglected in the remainder of the study.

The annual mean carbon subduction is therefore composed of three main components: a wind-induced Ekman transport; a mean geostrophic transport; and an eddy-induced transport. We compute these fluxes as follow[17]:

$$\overline{C_{subduction}} = (\overline{S_{ek}} \cdot \overline{C} + \overline{S_{geo}} \cdot \overline{C} + \overline{S_{eddy}} \cdot \overline{C}) \quad (3a)$$

where:

$$\overline{S_{ek}} = curl\left(\frac{\overline{\tau}}{\rho f}\right) \quad (3b)$$

$$\overline{S_{geo}} = \nabla \cdot (\overline{\mathbf{u}_{geo}} \cdot \overline{H_{max}}) \quad (3c)$$

$$\overline{S_{eddy}} = \nabla \cdot [\kappa \cdot \overline{\mathbf{s}}]_{z=H_{max}} \quad (3d)$$

f is the coriolis coefficient; H_{max} is the depth of the ventilated layer (that is, winter mixed-layer depth)[17]; τ is the wind stress estimated from satellite winds; ρ is the density of sea water; $\mathbf{u}_{geo}$ is the geostrophic velocity vector estimated from climatology strengthened with Argo data; κ is the mesoscale eddy diffusion intensity estimated from surface drifter trajectories[30]; and $\mathbf{s}$ is the slope of isopycnal (that is, $\overline{\mathbf{s}} = \nabla \overline{\rho}/\overline{\rho_z}$).

We compute equation (3) with an upwind-weighted scheme, which accounts for the dependence of the carbon transport on the sign of subduction: transport into the mixed layer from the interior uses the C_{ant} concentration 10 m below H_{max} and transport from the mixed layer to the interior uses the C_{ant} concentration in the mixed layer.

References

1. Raupach, M., Marland, G. & Ciais, P. Global and regional drivers of accelerating CO₂ emissions. *Proc. Natl Acad. Sci. USA* **104,** 10288–10293 (2007).
2. Le Quéré, C. *et al.* Trends in the sources and sinks of carbon dioxide. *Nature Geosci.* **2,** 831–836 (2009).
3. Doney, S. C., Lindsay, K., Caldeira, K. & Campin, J. Evaluating global ocean carbon models: The importance of realistic physics. *Glob. Biogeochem. Cycles* **18,** GB3017 (2004).
4. Matear, R. Effects of numerical advection schemes and eddy parameterizations on ocean ventilation and oceanic anthropogenic CO₂ uptake. *Ocean Model.* **3,** 217–248 (2001).
5. Sarmiento, J. L., Orr, J. C. & Siegenthaler, U. A perturbation simulation of CO₂ uptake in an Ocean General Circulation Model. *J. Geophys. Res.* **97,** 3621–3645 (1992).
6. Sabine, C. *et al.* The oceanic sink for anthropogenic CO₂. *Science* **305,** 367–371 (2004).
7. Ito, T., Woloszyn, M. & Mazloff, M. Anthropogenic carbon dioxide transport in the Southern Ocean driven by Ekman flow. *Nature* **463,** 80–83 (2010).
8. Mikaloff Fletcher, S. E. *et al.* Inverse estimates of anthropogenic CO₂ uptake, transport, and storage by the ocean. *Glob. Biogeochem. Cycles* **20,** GB2002 (2006).
9. Khatiwala, S., Primeau, F. & Hall, T. Reconstruction of the history of anthropogenic CO₂ concentrations in the ocean. *Nature* **462,** 346–349 (2009).
10. Rintoul, S., Hughes, C. & Olbers, D. The Antarctic circumpolar current system. *Ocean, Circulation and Climate* 271–302 (Academic, 2001).
11. McNeil, B., Tilbrook, B. & Matear, R. Accumulation and uptake of anthropogenic CO₂ in the Southern Ocean, south of Australia between 1968 and 1996. *J. Geophys. Res.* **106,** 31431–31445 (2001).
12. Iudicone, D. *et al.* Watermasses as a unifying framework for understanding the Southern Ocean carbon cycle. *Biogeosci. Discuss.* **7,** 3392–3451 (2010).
13. Le Quéré, C. *et al.* Saturation of the Southern Ocean CO₂ sink due to recent climate change. *Science* **316,** 1735–1738 (2007).
14. Lenton, A., Bopp, L. & Matear, R. Strategies for high-latitude northern hemisphere CO₂ sampling now and in the future. *Deep-Sea Res.* **56,** 523–532 (2009).
15. Lenton, A. & Matear, R. Role of the Southern Annular Mode (SAM) in Southern Ocean CO₂ uptake. *Glob. Biogeochem. Cycles* **21,** GB2016 (2007).
16. McNeil, B., Tilbrook, B. & Matear, R. Seasonal variations in DIC and d13CDIC in the subantarctic zone, South of Australia *Deep-Sea Res.* (in the press).
17. Sallée, J., Speer, K., Rintoul, S. & Wijffels, S. Southern Ocean thermocline ventilation. *J. Phys. Ocean.* **40,** 509–529 (2010).
18. Key, R., Kozyr, A., Sabine, C. & Lee, K. A global ocean carbon climatology: Results from Global Data Analysis Project (GLODAP). *Glob. Biogeochem. Cycles* **18,** GB4031 (2004).
19. Gruber, N., Sarmiento, J. L. & Stocker, T. F. An improved method for detecting anthropogenic CO₂ in the oceans. *Glob. Biogeochem. Cycles* **10,** 809–837 (1996).
20. Matsumoto, K. & Gruber, N. How accurate is the estimation of anthropogenic carbon in the ocean? An evaluation of the DC* method. *Glob. Biogeochem. Cycles* **19,** GB3014 (2005).
21. Alvarez, M. *et al.* Estimating the storage of anthropogenic carbon in the subtropical Indian Ocean: A comparison of five different approaches—OceanRep. *Biogeosciences* **6,** 681–703 (2009).
22. Lo Monaco, C., Goyet, C., Metzl, N., Poisson, A. & Touratier, F. Distribution and inventory of anthropogenic CO₂ in the Southern Ocean: Comparison of three data-based methods. *J. Geophys. Res.* **110,** C09S02 (2005).
23. Vázquez-Rodríguez, M. *et al.* Anthropogenic carbon distributions in the Atlantic Ocean: data-based estimates from the Arctic to the Antarctic. *Biogeosciences* **6,** 439–451 (2009).
24. Ito, T., Marshall, J. & Follows, M. What controls the uptake of transient tracers in the Southern Ocean. *Glob. Biogeochem. Cycles* **18,** GB2021 (2004).
25. Karleskind, P., Levy, M. & Mémery, L. Subduction of carbon, nitrogen, and oxygen in the northeast Atlantic. *J. Geophys. Res.* **116,** C02025 (2011).
26. Downes, S., Bindoff, N. & Rintoul, S. Impact of climate change on the subduction of mode and intermediate water masses in the Southern Ocean. *J. Clim.* **22,** 3289–3302 (2009).
27. Russell, J., Dixon, K., Gnanadesikan, A., Stouffer, R. & Toggweiler, J. The Southern Hemisphere westerlies in a warming world: Propping open the door to the deep ocean. *J. Clim.* **19,** 6382–6390 (2006).
28. Redi, M. Oceanic isopycnal mixing by coordinate rotation. *J. Phys. Ocean.* **12,** 1154–1158 (1982).
29. Solomon, H. On the representation of isentropic mixing in ocean circulation models. *J. Phys. Ocean.* **1,** 233–234 (1971).
30. Sallée, J., Speer, K., Morrow, R. & Lumpkin, R. An estimate of Lagrangian eddy statistics and diffusion in the mixed layer of the Southern Ocean. *J. Marine Res.* **66,** 441–463 (2008).
31. Cisewski, B., Strass, V. & Prandke, H. Upper-ocean vertical mixing in the Antarctic Polar Front Zone. *Deep-Sea Res.* **52,** 1087–1108 (2005).
32. Sallée, J., Speer, K. & Morrow, R. Response of the Antarctic Circumpolar Current to atmospheric variability. *J. Clim.* **21,** 3020–3039 (2008).

Author contributions

J-B.S. directed the analysis of the several data sets used here and shared responsibility for writing the manuscript. R.J.M., S.R.R. and A.L. participated in the data analysis and shared responsibility for writing the manuscript. All authors contributed to the final version of the manuscript.

Competing financial interests

The authors declare no competing financial interests.